The AppNL-G-F mouse model of Alzheimer's disease is refractory to regulatory T cell treatment

Lidia YSHII
KU Leuven: Katholieke Universiteit Leuven https://orcid.org/0000-0002-1988-6855
Loriana Mascali
KU Leuven: Katholieke Universiteit Leuven
Lubna Kouser
Babraham Institute
Pierre Lemaitre
KU Leuven University: Katholieke Universiteit Leuven
Marika Marino
KU Leuven: Katholieke Universiteit Leuven
James Dooley
Babraham Institute
Oliver Burton
Babraham Institute
Jeason Haughton
KU Leuven: Katholieke Universiteit Leuven
Zsuzsanna Callaerts-Vegh
KU Leuven: Katholieke Universiteit Leuven
Bart de Strooper
KU Leuven: Katholieke Universiteit Leuven
Matthew G Holt
KU Leuven: Katholieke Universiteit Leuven
Emanuela Pasciuto
KU Leuven: Katholieke Universiteit Leuven
Adrian Liston (✉ al989@cam.ac.uk)
KU Leuven: Katholieke Universiteit Leuven https://orcid.org/0000-0002-6272-4085

Research article

Keywords: Alzheimer's Disease, APP, mouse model, regulatory T cells, IL2

Posted Date: April 4th, 2022

DOI: https://doi.org/10.21203/rs.3.rs-1443371/v1

Abstract

Background: Alzheimer's Disease is a neurodegenerative disease with a neuroinflammatory component. Due to the multifunctional capacity of regulatory T cells to prevent and reverse inflammation, regulatory T cells have been proposed as a potential therapeutic in Alzheimer's Disease, either as a direct cell therapy or through the use of IL2 as a biologic to expand the endogenous population.

Methods: Here we characterize the longitudinal immunological changes occurring in T cells in the App^{NL-G-F} mouse model of Alzheimer's disease.

Results: Age-dependent immunological changes, in both the brain and periphery, occurred in parallel in both App^{NL-G-F} mice and control App^{NL} mice. As the endogenous IL2 axis was disturbed with age, we sought to determine the effect of IL2 supplementation on disease progression. Using a genetic model of IL2 provision in the periphery or in the brain, we found that expanding regulatory T cells in either location was unable to alter the progression of key pathological events or behavioral changes.

Conclusions: These results suggest that either the App^{NL-G-F} mouse model does not recapitulate key regulatory T cell-dependent process of Alzheimer's disease, or that regulatory T cell therapy is not a promising candidate for APP-mutation-driven Alzheimer's disease.

Background

Alzheimer's disease (AD) is the most common neurodegenerative disease and is characterized by β-amyloid peptide (Aβ) plaques and tau tangles, complemented by astrogliosis and activated microglia [1]. However, growing evidence suggests that the amyloid cascade alone cannot recapitulate the pathogenesis of AD, indicating the involvement of other pathological processes [2]. In particular, in AD patients, T cell activation is observed in both the peripheral blood [3] and cerebral spinal fluid (CSF) [4], and T cell infiltration into the brain has been observed[5]. Moreover, AD risk variants are associated with both innate immune functions, and variants in HLA, responsible for antigen presentation to T cells [6, 7]. Further linkage to the adaptive immune system is suggested through the report of lower IL2 levels in the AD brain [8]. Taken together, inflammation is likely a fundamental player during AD progression, with infiltrating T cells a likely mediator of pathology [9].

With a potential pathophysiologic function for T cells, harnessing regulatory T cells (Tregs) has been proposed as a potential therapeutic approach. Tregs are multifunctional anti-inflammatory cells, capable of suppressing inappropriate immune activation[10]. The vast majority of research on Tregs has occurred in the peripheral context, where they increase the threshold for activation of conventional T cells. In the neurological context, this potentially allows Tregs to prevent the priming of neurodestructive T cells[11, 12]. Recently, there has been a growing appreciation that a small population of Tregs are resident in the brain tissue of mice and humans, even in the healthy context [13]. These cells can produce neurotrophic factors, such as brain-derived neurotrophic factor (BDNF) [14] and anti-inflammatory factors, such as

amphiregulin, suppressing neurotoxic astrogliosis [15]. We recently demonstrated that expansion of the brain-resident Treg population, through the local provision of the key survival factor interleukin 2 (IL2) was neuroprotective in mouse models of traumatic brain injury, stroke and multiple sclerosis[16]. Together, these findings suggest that brain Tregs can play a protective role in central nervous system-related inflammation.

We considered therefore Tregs as a potential therapeutic target in AD, either through direct cell therapy or through the supplementation of the endogenous population with the survival factor IL2 [17]. The role of Tregs in AD is, however, highly contested, with different studies proposing either a protective effect of Tregs [18], a detrimental effect of Tregs [19, 20] or no effect of Tregs [21] on plaque load. Increased numbers of Tregs have been correlated with reduced microglia activation and production of inflammatory cytokines [18], but the effect of Treg interaction on phagocytic capacity of microglia is debated [20, 21]. The beneficial effect of Tregs on the cognitive performance of AD mouse model is, however, complementary [8, 18, 21]. Confounding these studies is a potential divergence in the net effect of peripheral or brain-resident Tregs [19], with most studies using a methodology that does not allow for discrimination. In order to independently test the potential benefit of therapeutic IL2-mediated Treg expansion, and to distinguish between the roles of peripheral and brain resident Tregs, here we used two specific methods for the genetic delivery of IL2 expression allowing the systemic- or brain-specific expansion of Tregs in the App^{NL-G-F} mouse model of Alzheimer's Disease. Expansion of the Treg population was observed as expected: however, no substantial amelioration of plaque formation or cognitive decline was observed. These results suggest the pathology of the App^{NL-G-F} mouse model is refractory to Treg treatment, either through systemic or brain-directed expansion.

Methods

Mice

Human amyloid precursor protein (hAPP) knock-in (KI) mice containing the Swedish, Iberian, and Arctic mutations included (App^{NL-G-F}) were used on a C57BL/6 J background [22]. Foxp3-Cre transgenic mice [23] and αCamKII-CreERT2 transgenic mice [24] were used on the C57BL/6 background. RosaIL2 mice were generated through the insertion of a cassette containing a floxed-STOP sequence followed by an IL2-IRES-GFP sequence into the Rosa26 locus, using the endogenous Rosa26 promoter [25], and were used on the C57BL/6 background. Both male and female mice were used in this study. Mice were age-matched and tested at 2, 4, and 9 months of age. Tamoxifen (Sigma T5648) was solubilized in corn oil (Sigma) at 10 mg/ml. Five to seven weeks old αCamKII-CreERT2 mice were injected 3 times, via intraperitoneal injection, at 48 h intervals using a dose of 100 mg/kg body weight. Mice were housed under SPF conditions, under a 12-hour light/dark cycle in a temperature and humidity-controlled room with *ad libitum* access to food and water. All animal procedures were approved by the KU Leuven Animal Ethics Committee (P124/2019), and were consistent with European guidelines.

Flow cytometry

Mice were deeply anaesthetized with intraperitoneal injection of a ketamine (87 mg/kg), xylazine (13 mg/kg) mixture. Blood was collected from the right ventricle prior to transcardial perfusion with ice cold PBS, and further processed through red blood cell lysis. Single-cell suspensions from lymphoid organs were prepared by mechanical dissociation; single-cell suspensions from brain tissue were prepared by digestion for 30 minutes at 37ºC with 1 mg/ml collagenase IV (Thermo Fisher), 300 µg/ml hyaluronidase (Sigma-Aldrich) and 40 µg/ml DNase I (Sigma-Aldrich) in RPMI 1640 supplemented with 2 mM $MgCl_2$, 2mM $CaCl_2$, 20% FBS and 2 mM HEPES (Gibco), followed by mechanical disruption, filtration (through 100 µm mesh) and enrichment for leukocytes by gradient centrifugation (40% Percoll GE Healthcare, 600 x g, 10 min). Non-specific binding was blocked using 2.4G2 supernatant. To assess intracellular cytokine production, cells were cultured for 4h in the presence of phorbol mysristate acetate (1 µg/ml, Sigma-Aldrich), ionomycin (1 µg/ml, Sigma-Aldrich), and brefeldinA (BD). Cells were fixed and permeabilized with the eBioscience Foxp3 staining kit (eBioscience). Cellular phenotypes were assessed using high parameter flow cytometry panels, containing markers to identify cell types and markers to assess activation states. Data were acquired on a BD FACSymphony, with panels covering (i) CD45, CD4, CD8, CD3, CD19, NK1.1, Foxp3, eBioscience™ Fixable Viability Dye eFluor™ 780, CD103, CD62L, CD25, Neuropilin, ST2, PD-1, KLRG1, Helios, CD69, ICOS, CD44, and Ki67 or (ii) CCR6, CD80, TCRγδ, CD45, Foxp3, MHCII, eBioscience™ Fixable Viability Dye eFluor™ 780, IL1β, CD25, Ly6G, ST2, CX3CR1, PD-L1, TNF, CD44, Ki67, CD4, Ly6C, TrkB, CD19, CD69, CD8α, LAMP1, CD64, CD11b, CD3, or (iii) Foxp3, eBioscience™ Fixable Viability Dye eFluor™ 780, IL5, IL6, IL17, CD4, IFNγ, CD8α, TNFα, CD3, Amphiregulin, IL10, IL4, CD11b, CD19, GM-CSF, TCRγδ, pro-IL1β, TCRβ, IL2, NK1.1. For brain panels, cells obtain from the whole brain were analysed. Data was compensated using AutoSpill [26].

tSNE, FlowSOM and heatmap analysis were performed in RStudio (version 1.4.1717) using an in-house script [26]. FlowSOM clusters are formed based on multi-marker similarity in a non-supervised manner. Clusters were annotated based on post-clustering comparison of marker expression, aligning the unique marker profile of each cluster to literature-based nomenclature. Key annotations for T cell clusters included CD4 naïve ($CD3^+CD4^+CD62L^{hi}CD44^{low}$), CD4 activated ($CD3^+CD4^+CD62L^{low}CD44^{high}$), CD4 memory ($CD3^+CD4^+CD62L^{hi}CD44^{high}$), Tregs ($CD3^+CD4^+Foxp3^+$), CD8 naïve ($CD3^+CD8^+CD62L^{hi}CD44^{low}$), CD8 activated ($CD3^+CD8^+CD62L^{low}CD44^{high}$), and CD8 memory ($CD3^+CD8^+CD62L^{hi}CD44^{high}$).

Immunostaining

Mice were deeply anaesthetized using intraperitoneal injection of a ketamine (87 mg/kg) / xylazine (13 mg/kg) mixture and transcardially perfused with PBS followed by 4% buffered formalin solution. The brain was removed and fixed in 10% buffered formalin solution overnight and stored in 30% sucrose until preservation in tissue freezing medium (Shandon™ Cryomatrix™ embedding resin, Thermo Scientific), and stored at -80°C. Sections (50 µm) were washed 15 minutes in 50 mM NH_4Cl/PBS and pre-blocked with 10% normal donkey serum in 0.5% Triton-X-100/PBS for 1h at room temperature. Sections were incubated overnight at 4ºC with primary antibodies directed against Iba1 (1:1000, 014-19741, Wako) and 6E10 Abeta (1:1000, SIG-39320-1000, Covance Signet). Subsequently, the sections were incubated for 90 minutes at room temperature with appropriate fluorophore-conjugated secondary antibodies (Thermo

Scientific). After each antibody incubation, slices were washed 3 times for 10 minutes with 0.1% Triton-X-100/PBS. All sections were incubated with DAPI (1:1000) for 15 min before final mounting on microslide slides using ProlongGold (Invitrogen). Images were obtained using a Nikon A1R Eclipse Ti confocal (Plan Apo 20X), or a Zeiss Axioscan Z.1 slide-scanner (20X Plan-Apochromat/NA 0.8) equipped with a Hamamatsu Orca Flash 4.0 V3 camera. Image processing was performed using ImageJ (https://imagej.nih.gov/ij/download.html).

ELISA

Soluble and insoluble fractions of Aβ were extracted from cortex and hippocampus, as previously described [27] 1368. The total protein content of the samples containing the soluble and insoluble Aβ fractions was determined using a modified Lowry-Peterson assay. The concentration of $A\beta_{1-40}$ or $A\beta_{1-42}$ in tissue samples was determined using standard sandwich ELISAs. Monoclonal antibodies JRFcAβ40/28 and JRFcAβ42/26, which recognize the C-terminal ends of Aβ species terminating at amino acids 40 or 42 respectively, were used for capture. HRP-conjugated JRFAβN/25 antibody, which recognizes the first seven N-terminal amino acids of human Aβ, was used as a detection antibody. Synthetic human $A\beta_{1-40}$ and $A\beta_{1-42}$ peptides were used to generate standard curves. Antibodies were kindly provided by Johnson and Johnson. Absorbance was measured at 450 nm in a Perkin Elmer EnVision 2103 Multilabel reader.

Morris Water Maze

Morris Water Maze behavioral experiments were performed in 9 months old mice. Mice were habituated to their new environment for at least 7 days and tests were conducted during the light phase of their activity cycle. Tests were performed and analyzed by an observer blind to the experimental group. Spatial learning and cognitive flexibility were tested in the hidden platform Morris Water Maze. A circular pool (150 cm diameter) was filled with opacified (0.01% Acusol OP301, Dow Chemicals) water (26 ± 1°C). The platform (15 cm diameter) was hidden 1 cm underneath the surface of the water. For spatial learning, the mice were trained for 10 days to a fixed platform position [28, 29]. To evaluate reference memory, probe trials (100 seconds) were conducted on days 6 and 11 during acquisition learning. During probe trials, floater mice were excluded. The escape platform was removed from the pool and mice were allowed to explore the maze for 100 seconds. Swim paths were tracked with Ethovision software (Noldus).

Statistics

Comparisons between two groups were performed using unpaired two-tailed Student's t tests. Post hoc Holm's or Sidak's multiple comparisons tests were performed, when required. Two-way ANOVA was used, when appropriate. The value of n reported within figure legends represents the number of animals. Values are represented as mean ± SEM, with differences considered significant when $p < 0.05$.

Results

Cumulative age-dependent changes in the peripheral and brain-resident immunological compartments in AD mice

Growing evidence suggests T cell involvement in AD pathogenesis [9]. We performed in depth phenotyping by high dimensional flow cytometry of the T cell compartment in the App^{NL-G-F} and in the control App^{NL} strain, and at different stages of disease progression. Specifically, before plaques deposition (2 months), after plaques deposition (4 months), and when cognitive impairment is detectable (9 months) in the App^{NL-G-F} [22]. We first assessed the peripheral compartment, represented by the spleen, blood and the draining cervical lymph nodes (cLN). Classification of T cell populations by tSNE analysis (**Supplementary Fig. 1**), found a decline in naïve CD4 T cells with age across spleen and blood, consistent in both the App^{NL} and App^{NL-G-F} mice (Fig. 1A). Naïve CD4 T cells were displaced by increased CD8 T cells, and, in some mice, large increases in memory CD4 T cells (Fig. 1A). We next investigated the expression of key activation markers (Fig. 1B) and cytokine production (Fig. 1C), in each of the conventional CD4 T cell (**Supplementary Fig. 2**), Treg (**Supplementary Fig. 3**) and CD8 T cell (**Supplementary Fig. 4**) lineages. While most phenotypes remained stable with age, several consistent changes observed, including a reduction in CD25 expression in Tregs (Fig. 1B, D), an increase in amphiregulin production by Tregs (Fig. 1C, D) and elevated TNF production by CD8 T cells, with a peak at 4 months on App^{NL-G-F} mice (Fig. 1C,D). Changes were largely mirrored between App^{NL} and App^{NL-G-F} mice; however, cytokine production was inconsistent between the two strains, with App^{NL-G-F} mice demonstrating increased IL2 production by CD4 T cells and TNF production by CD8 T cells in the cLN at four months of age, and a slight decrease in IL2 production by CD4 T cells at 9 months in the spleen (Fig. 1D). These results suggest that App^{NL-G-F} mice undergo predictable changes in the T cell compartment, driven largely by age rather than the that App^{NL-G-F} mutations.

We next assessed the changes to T cell populations in the brain tissue. Major T cell subsets (Fig. 2A) were quantified, demonstrating an age-dependent displacement of activated CD4 T cells and Tregs by activated CD8 T cells (Fig. 2B). These effects were age-dependent rather than genotype-dependent, with few changes observed between App^{NL} and App^{NL-G-F} mice (**Supplementary Fig. 5**). At the level of activation marker expression (Fig. 2C), the only consistent change was in the age-dependent increase of CD44 expression on CD8 T cells (Fig. 2D), reflecting the increase in the activated CD8 T cell population. Together, these results do not support a model of App^{NL-G-F} expression actively driving major immunological changes in the T cell compartment. However, the age-dependent changes are consistent with an alternative model, whereby the shifts in the T cell population in the older mouse (9 months) are permissive for a neuroinflammatory reaction precipitated by App^{NL-G-F} expression and subsequent Aβ accumulation. Under this latter model, App^{NL-G-F} expression in the young brain may be quiescent due to a protective immunological context, however normal “healthy” changes in phenotypes such as the IL2-Treg access (lower IL2 production by conventional CD4 T cells and lower CD25 expression on Tregs in the draining lymph nodes, lower Treg frequency in the brain tissue) may provide the immunological environment that allows App^{NL-G-F} expression to become pathogenic.

Peripherally-biased expansion of Treg numbers via IL2 self-sufficiency does not alter pathology of AD

Our observation that the major identified age-dependent change observed in App^{NL} and App^{NL-G-F} mice is in the IL2-Treg axis is consistent with prior reports that IL2 or Treg treatment can prevent aspects of neurodegenerative phenotypes in AD model mice [8]. A limitation of prior studies is that treatment with either IL2 or Treg creates global changes, which do not allow a distinction between the role of Tregs in peripheral organs (e.g., regulation of priming events in the spleen or draining lymph nodes) versus the role of Tregs in the brain itself (e.g. promoting repair or creating an anti-inflammatory environment) to be determined. To separate these effects, we used a Cre-inducible IL2 transgene, allowing low levels of IL2 production to be initiated in a cell-dependent manner [25]. First, we used a *Foxp3*-Cre transgene to drive IL2 production in Tregs ($Foxp3^{Cre}$RosaIL2 mice). By employing such a system, we effectively circumvent the normal dependence of Treg expansion on exogenous IL2 provision [25]. By crossing $Foxp3^{Cre}$RosaIL2 mice to either App^{NL} and App^{NL-G-F} mice (Fig. 3A), we generated a Treg-enriched environment in both lines (Fig. 3C**)**. Due to the low levels of IL2 produced in this system, the non-Treg compartment remains unchanged, in both the periphery (spleen, blood, cLN) and brain (Fig. 3B). The activation profile of both conventional CD4 and CD8 T cells remained unchanged by IL2 expression, in both periphery (**Supplementary Figs. 6–7**) and brain (**Supplementary Fig. 8**). By contrast, the Treg population increased in an age-dependent manner, with peripheral Tregs increasing by roughly 2-fold, 5-fold and 10-fold at 2, 4 and 9 months of age, respectively (Fig. 3C). The expansion in the numbers of circulating Tregs occurs at the cost of the tissue-resident population [16]. This results in a substantial delay in Treg expansion in the brain tissue, with increases not observed until the mice are 9 months old (Fig. 3D). This expansion process did not, however, substantially alter the activation profile of Tregs in either the brain (**Supplementary Fig. 8**) or periphery (**Supplementary Fig. 9**) at the 2, 4, and 9-month time-points. The system thereby provided App^{NL-G-F}-IL2 mice where dominant Treg expansion occurred in peripheral tissues, but not exclusively. Despite the substantial and early increase in peripheral Treg numbers in App^{NL-G-F}-IL2 mice, no change was observed in guanidine extracted Aβ (40, 42) measured using ELISA (Fig. 3E), or in plaque accumulation measured by immunofluorescence (Fig. 3F). Measurement of spatial learning in the Morris Water Maze showed clear cognitive decline in 9 month-old App^{NL-G-F} mice, with reduced preference for the target quadrant after learning (Fig. 3G). App^{NL-G-F}-IL2 mice showed only a minor effect no improvement in spatial cognitive learning over App^{NL-G-F} mice (Fig. 3G), demonstrating that elevated peripheral Treg numbers were unable to prevent the cognitive decline observed in the App^{NL-G-F} model.

Brain-specific expansion of Treg numbers via brain-delivery of IL2 does not alter pathology of AD

Finally, we performed the reciprocal test, analyzing the effect of specific expansion of brain Tregs on APP-mediated pathology. Here we used the $CamKII^{Cre}$ allele to trigger activation of the IL2 transgene

specifically in CamKII^{+} neurons, previously demonstrated to drive a brain-specific expansion of Tregs [16]. By crossing CamKII^{Cre}RosaIL2 mice to *App*$^{NL-G-F}$ mice, we generated a brain-specific IL2 expression system in AD model mice (Fig. 4A). Comparing *App*$^{NL-G-F}$-CamKII^{L2} mice to *App*$^{NL-G-F}$ mice, no changes were apparent in the frequency of conventional T cell populations, in either the peripheral tissues (blood, spleen, cLN) or the brain (Fig. 4B). Likewise, activation profiles remained unchanged in both periphery (**Supplementary Fig. 10–11**) and brain (**Supplementary Fig. 12**). Treg frequency, by contrast, was normal in peripheral tissues, but was significantly increased (~ 5-fold) in the brain, from 2 months of age (Fig. 4C). Activation markers remained constant with IL2 treatment, demonstrating that the effect of IL2 was numerical expansion rather than alteration of phenotype (**Supplementary Fig. 12–13**). This creates a context where we have a brain-specific increase in IL2 and Tregs from a young age, in the presence of a humanized, mutated *App* allele, designed to drive AD-like pathogenesis. Despite Tregs being elevated in the brain throughout the period of amyloid deposition, no significant changes were detected in the amount of insoluble $A\beta_{1-40}$ and $A\beta_{1-42}$ in the whole cortex (Fig. 4D). Likewise, with regard to the development of behavioral abnormalities, *App*$^{NL-G-F}$-CamKII^{L2} mice showed no improvement in the Morris Water Maze compared to *App*$^{NL-G-F}$ mice **(**Fig. 4E). Together with the results from the *App*$^{NL-G-F}$-IL2 mice, this suggests that neither peripheral-biased nor brain-specific expansion of Tregs substantially alters pathology in the *App*$^{NL-G-F}$ AD mouse model.

Discussion

Unlike previous studies reporting either a protective effect of Tregs [8, 18] or a detrimental effect of Tregs [19, 20, 30] on disease progression in AD model mice, here we observed no effect of either peripheral-biased Treg expansion or brain-specific Treg expansion on cognitive decline and Amyloid beta aggregates. Of the potential explanations for the discrepancy in results, one is the use of different models of AD[31]. Previous studies on the role of Tregs on AD pathology have been performed in mouse models that overexpress the Aβ precursor protein (APP) in combination with different familial AD associated mutations, however multiple different models have been used. Alves *et al*, reporting a protective effect, used the APP/PS1 strain, which combine the Swedish APP mutation with the L166P PSEN1 mutation [8] and Baek *et al*, used the the 3xTg-AD mice containing three mutations associated with familial Alzheimer's disease (APP Swedish, MAPT P301L, and PSEN1 M146V) [18]. Two studies have reported detrimental effects of Tregs, using the APP/PS1 mice [20], the 5XFAD mice [19], containing APP transgenes covering 5 AD-linked mutations and the L286V mutation in PSEN1. Finally, the Dansokho study, which, like our study, reported no impact of Tregs on Aβ plaque load, used the APP/PS1 mice [21] and only a minor effect on behavioral tasks. Our study is the first to test the role of Tregs in the *App*$^{NL-G-F}$ model. Unlike the other APP transgenic models previously used, *App*$^{NL-G-F}$ is a single knock-in with expression driven by the endogenous promoter, and doers not harbor mutation in the PSEN1 gene, reducing artefacts caused by over-expression or off-target processing [22]. This is of particular importance in ascertaining the function of the immune system in AD processes, as human transgenic PSEN1 was found in splenocytes and off target processing could create a role for T cells in the model

that does not represent the physiological process occurring in patients [32]. However, the presence of multiple mutations in the same APP gene, not observed in human patients, could in principle interact with each other in some cases that may not accurately represent clinical AD.

While the discrepancy between our result and previous studies observing an effect of Tregs may be due to the transgenic model used, it is notable that three separate studies using the APP/PS1 model demonstrated no effect, a beneficial effect and a detrimental effect of Tregs on plaque load [8, 20, 21]. These results are unlikely to be due to strain differences, and may reflect the diversity of approaches used to test the role of Tregs. Several studies have used depletion systems, either through PC61 anti-CD25 antibody or using the diphtheria toxin system in transgenic mice [19, 21]. These systems result in large-scale immune activation in addition to Treg depletion, and depending on the kinetics of treatment resurgent Treg number can even be locally elevated [19], confounding interpretation. Baek *et al* used the direct adoptive transfer of Tregs [19], which can transiently raise Treg numbers, although niche-sensing systems cause retraction of an overly abundant Treg population [17]. Finally, several studies have expanded endogenous Tregs, either through the provision of all-trans retinoic acid [19, 20] or IL2 [8, 21]. These approaches have the advantage of being therapeutically translatable, however there are limits to the degree to which mechanism of activity can be inferred. While all-trans retinoic acid expands Treg numbers [33], it has numerous effects on other aspects of the immune system [34] and nervous system, including amyloid processing[35]. Likewise, IL2 at low doses is a selective survival factor for Tregs, however at higher doses other cell types, including CD8 T cells, respond. Our study has the advantage that IL2 is being supplemented at doses low enough that only Tregs respond[16], with the cell lineage-mediated production of IL2 allowing segregation of peripheral and brain Treg functions.

Conclusions

At face value, the conclusions of our study do not support the use of IL2 or Treg therapy in AD. It is important, however, to consider that the lack of response may be driven by the limitations of the mouse model. *App*$^{NL-G-F}$ mice only replicate a single aspect of AD disease progression, that driven by plaque formation, and can be considered to be models of preclinical AD, rather than of AD. *App*$^{NL-G-F}$ mice are therefore a useful preclinical model to study processes such as glial responses to amyloid stress, but lack other important aspects of AD. The *App*$^{NL-G-F}$ KI mice do, however, upregulate multiple neuroinflammation-related genes in common with AD patients genes (*C4a/C4b, Cd74, Ctss, Gfap, Nfe212, Phyhd1, S100b, Tf, Tgfbr2* and *Vim*) and AD risk factor genes (A*bi3, Apoe, Bin2, Cd33, Ctsc, Dock2, Fcer1g, Frmd6, Hck, Inpp5D, Ly86, Plcg2, Trem2* and *Tyrobp*)[22, 30, 36]. Importantly, the mice do not exhibit tau pathology or neurodegeneration [22], a key phenotype in patients [37], suggesting that can be useful as preclinical AD model to investigate the pathological role of amyloid-associated neuroinflammation The lack of tau pathology is particularly pertinent as studies of human AD postmortem brains indicates that T cell infiltration correlates with tau pathology rather than with amyloid plaques [38]. The APP^{NLGF} mouse model also progresses independent of the adaptive immune system, in Rag-deficient mice [39], contradicting genetic association of human AD with adaptive immunity [6, 7]. We

therefore provide the more nuanced conclusion that the current results do not support the use of IL2 or Treg therapy in AD patients where the primary driver is APP, without discounting potential efficacy in AD patients where tau pathology is a primary driver. Indeed, we have previously demonstrated that brain-specific delivery of IL2 prevents cognitive decline in APP-independent mouse models of traumatic brain injury [16] and old age [40], validating the use of IL2 or Treg therapy in dementia more generally. We therefore echo the call that any potential clinical trials should take into account the heterogeneity of AD disease, with stratification based on genotype and tau pathology increasing the potential for efficacious responses.

Abbreviations

AD: Alzheimer's disease

APP: Amyloid precursor protein

AREG: Amphiregulin

Aβ: Amyloid beta peptide

BDNF: Brain-derived neurotrophic factor

cLN: Cervical lymph node

CSF: Cerebral spinal fluid

ELISA: Enzyme linked immunosorbent assays

FlowSOM: Flow self-organizing map

HLA: Human leukocyte antigen

IL2: Interleukin 2

KI: Knock-in

PSEN1: Presenilin 1

TNF: Tumor necrosis factor

Tregs: Regulatory T cells

tSNE: t-distributed stochastic neighbor embedding

Declarations

Ethics approval

All animal experiments were conducted according to protocols approved by the local Animal Ethical Committee of the KU Leuven (P124/2019) which adheres to local governmental and EU guidelines.

Consent for publication

All authors read and approved the final manuscript.

Availability of data and materials

The datasets used and/or analyzed during the current study are available from the corresponding author on reasonable request.

Competing interests

The authors report no competing interests.

Funding

The work was supported by the Alzheimer's Association AARG (to A.L.), the VIB, an ERC Consolidator Grant TissueTreg (to A.L.), an ERC Proof of Concept Grant TreatBrainDamage (to A.L.), FWO Research Grant 1503420N (to EP), an SAO-FRA pilot grant (20190032, to E.P.), an ERC Starting Grant AstroFunc (to M.G.H.), the ERC Proof of Concept Grant AD-VIP (to M.G.H.), FWO Research Grant 1513616N (to M.G.H.), Thierry Latran Foundation Grant SOD-VIP (to M.G.H.), SAO-FRA pilot grant (14006) (to M.G.H.), ERNAET Chair NCBio (to M.G.H.), and the Biotechnology and Biological Sciences Research Council through Institute Strategic Program Grant funding BBS/E/B/000C0427 and BBS/E/B/000C0428, and the Biotechnology and Biological Sciences Research Council Core Capability Grant to the Babraham Institute. E.P. was supported by a fellowship from the FWO.

Authors'contributions

AL conceived the study and wrote the manuscript. LY and EP designed the study and wrote the manuscript. LY, LM, LK, PL, MM, JD, OB, JH, ZC-V, and EP performed experiments. MGH participated in discussions and manuscript preparation. All authors read and approved the final manuscript.

Acknowledgements

The authors acknowledge the important contributions of the KUL FACS Core.

References

1. De Strooper B, Karran E. The Cellular Phase of Alzheimer's Disease. Cell. 2016;164:603–15.
2. Herrup K. The case for rejecting the amyloid cascade hypothesis. Nat Neurosci. 2015;18:794–9.

3. Saresella M, Calabrese E, Marventano I, Piancone F, Gatti A, Calvo MG, Nemni R, Clerici M. PD1 negative and PD1 positive CD4 + T regulatory cells in mild cognitive impairment and Alzheimer's disease. J Alzheimers Dis. 2010;21:927–38.
4. Gate D, Saligrama N, Leventhal O, Yang AC, Unger MS, Middeldorp J, Chen K, Lehallier B, Channappa D, De Los Santos MB, et al. Clonally expanded CD8 T cells patrol the cerebrospinal fluid in Alzheimer's disease. Nature. 2020;577:399–404.
5. Togo T, Akiyama H, Iseki E, Kondo H, Ikeda K, Kato M, Oda T, Tsuchiya K, Kosaka K. Occurrence of T cells in the brain of Alzheimer's disease and other neurological diseases. J Neuroimmunol. 2002;124:83–92.
6. Chouraki V, Seshadri S. Genetics of Alzheimer's disease. Adv Genet. 2014;87:245–94.
7. Jonsson T, Stefansson H, Steinberg S, Jonsdottir I, Jonsson PV, Snaedal J, Bjornsson S, Huttenlocher J, Levey AI, Lah JJ, et al. Variant of TREM2 associated with the risk of Alzheimer's disease. N Engl J Med. 2013;368:107–16.
8. Alves S, Churlaud G, Audrain M, Michaelsen-Preusse K, Fol R, Souchet B, Braudeau J, Korte M, Klatzmann D, Cartier N. Interleukin-2 improves amyloid pathology, synaptic failure and memory in Alzheimer's disease mice. Brain. 2017;140:826–42.
9. Heneka MT, Carson MJ, El Khoury J, Landreth GE, Brosseron F, Feinstein DL, Jacobs AH, Wyss-Coray T, Vitorica J, Ransohoff RM, et al. Neuroinflammation in Alzheimer's disease. Lancet Neurol. 2015;14:388–405.
10. Liston A, Gray DH. Homeostatic control of regulatory T cell diversity. Nat Rev Immunol. 2014;14:154–65.
11. Koutrolos M, Berer K, Kawakami N, Wekerle H, Krishnamoorthy G. Treg cells mediate recovery from EAE by controlling effector T cell proliferation and motility in the CNS. Acta Neuropathol Commun. 2014;2:163.
12. Kramer TJ, Hack N, Bruhl TJ, Menzel L, Hummel R, Griemert EV, Klein M, Thal SC, Bopp T, Schafer MKE. Depletion of regulatory T cells increases T cell brain infiltration, reactive astrogliosis, and interferon-gamma gene expression in acute experimental traumatic brain injury. J Neuroinflammation. 2019;16:163.
13. Pasciuto E, Burton OT, Roca CP, Lagou V, Rajan WD, Theys T, Mancuso R, Tito RY, Kouser L, Callaerts-Vegh Z, et al. Microglia Require CD4 T Cells to Complete the Fetal-to-Adult Transition. Cell. 2020;182:625–40 e624.
14. Kerschensteiner M, Gallmeier E, Behrens L, Leal VV, Misgeld T, Klinkert WE, Kolbeck R, Hoppe E, Oropeza-Wekerle RL, Bartke I, et al. Activated human T cells, B cells, and monocytes produce brain-derived neurotrophic factor in vitro and in inflammatory brain lesions: a neuroprotective role of inflammation? J Exp Med. 1999;189:865–70.
15. Ito M, Komai K, Mise-Omata S, Iizuka-Koga M, Noguchi Y, Kondo T, Sakai R, Matsuo K, Nakayama T, Yoshie O, et al. Brain regulatory T cells suppress astrogliosis and potentiate neurological recovery. Nature. 2019;565:246–50.

16. Yshii L, Pasciuto E, Bielefeld P, Mascali LG, Lemaitre P, Marino M, Dooley J, Kouser L, Verschoren S, Lagou V, et al: **Astrocyte-targeted gene delivery of interleukin 2 specifically increases brain-resident regulatory T cell numbers and protects against pathological neuroinflammation** *BioRxiv* 2022.
17. Pierson E, Simmons SB, Castelli L, Goverman JM. Mechanisms regulating regional localization of inflammation during CNS autoimmunity. Immunol Rev. 2012;248:205–15.
18. Baek H, Ye M, Kang GH, Lee C, Lee G, Choi DB, Jung J, Kim H, Lee S, Kim JS, et al. Neuroprotective effects of CD4 + CD25 + Foxp3 + regulatory T cells in a 3xTg-AD Alzheimer's disease model. Oncotarget. 2016;7:69347–57.
19. Baruch K, Rosenzweig N, Kertser A, Deczkowska A, Sharif AM, Spinrad A, Tsitsou-Kampeli A, Sarel A, Cahalon L, Schwartz M. Breaking immune tolerance by targeting Foxp3(+) regulatory T cells mitigates Alzheimer's disease pathology. Nat Commun. 2015;6:7967.
20. Yang Y, He Z, Xing Z, Zuo Z, Yuan L, Wu Y, Jiang M, Qi F, Yao Z. Influenza vaccination in early Alzheimer's disease rescues amyloidosis and ameliorates cognitive deficits in APP/PS1 mice by inhibiting regulatory T cells. J Neuroinflammation. 2020;17:65.
21. Dansokho C, Ait Ahmed D, Aid S, Toly-Ndour C, Chaigneau T, Calle V, Cagnard N, Holzenberger M, Piaggio E, Aucouturier P, Dorothee G. Regulatory T cells delay disease progression in Alzheimer-like pathology. Brain. 2016;139:1237–51.
22. Saito T, Matsuba Y, Mihira N, Takano J, Nilsson P, Itohara S, Iwata N, Saido TC. Single App knock-in mouse models of Alzheimer's disease. Nat Neurosci. 2014;17:661–3.
23. Zhou X, Jeker LT, Fife BT, Zhu S, Anderson MS, McManus MT, Bluestone JA. Selective miRNA disruption in T reg cells leads to uncontrolled autoimmunity. J Exp Med. 2008;205:1983–91.
24. Madisen L, Zwingman TA, Sunkin SM, Oh SW, Zariwala HA, Gu H, Ng LL, Palmiter RD, Hawrylycz MJ, Jones AR, et al. A robust and high-throughput Cre reporting and characterization system for the whole mouse brain. Nat Neurosci. 2010;13:133–40.
25. Whyte CE, Singh K, Burton OT, Aloulou M, Moudra A, Roca CP, Naranjo F, Lombard-Vadnais F, Hochepied T, Halim T, et al: **Context-dependent effects of IL-2 rewire immunity into distinct cellular circuits.** *BioRxiv* 2021.
26. Roca CP, Burton OT, Neumann J, Tareem S, Whyte CE, Humblet-Baron S, Liston A. **A Cross Entropy test allows quantitative statistical comparison of t-SNE and UMAP representations**. ArXivorg 2021, 1.
27. Marino M, Zhou L, Rincon MY, Callaerts-Vegh Z, Verhaert J, Wahis J, Creemers E, Yshii L, Wierda K, Saito T, et al: **AAV-mediated delivery of an anti-BACE1 VHH alleviates pathology in an Alzheimer's disease model**. EMBO Mol Med 2022.
28. Callaerts-Vegh Z, Beckers T, Ball SM, Baeyens F, Callaerts PF, Cryan JF, Molnar E, D'Hooge R. Concomitant deficits in working memory and fear extinction are functionally dissociated from reduced anxiety in metabotropic glutamate receptor 7-deficient mice. J Neurosci. 2006;26:6573–82.
29. D'Hooge R, De Deyn PP. Applications of the Morris water maze in the study of learning and memory. Brain Res Brain Res Rev. 2001;36:60–90.

30. Sala Frigerio C, Wolfs L, Fattorelli N, Thrupp N, Voytyuk I, Schmidt I, Mancuso R, Chen WT, Woodbury ME, Srivastava G, et al. The Major Risk Factors for Alzheimer's Disease: Age, Sex, and Genes Modulate the Microglia Response to Abeta Plaques. Cell Rep. 2019;27:1293–306 e1296.
31. Sasaguri H, Nilsson P, Hashimoto S, Nagata K, Saito T, De Strooper B, Hardy J, Vassar R, Winblad B, Saido TC. APP mouse models for Alzheimer's disease preclinical studies. EMBO J. 2017;36:2473–87.
32. Radtke F, Fasnacht N, Macdonald HR. Notch signaling in the immune system. Immunity. 2010;32:14–27.
33. Mucida D, Park Y, Kim G, Turovskaya O, Scott I, Kronenberg M, Cheroutre H. Reciprocal TH17 and regulatory T cell differentiation mediated by retinoic acid. Science. 2007;317:256–60.
34. Hao X, Zhong X, Sun X. The effects of all-trans retinoic acid on immune cells and its formulation design for vaccines. AAPS J. 2021;23:32.
35. Koryakina A, Aeberhard J, Kiefer S, Hamburger M, Kuenzi P. Regulation of secretases by all-trans-retinoic acid. FEBS J. 2009;276:2645–55.
36. Latif-Hernandez A, Sabanov V, Ahmed T, Craessaerts K, Saito T, Saido T, Balschun D. The two faces of synaptic failure in App(NL-G-F) knock-in mice. Alzheimers Res Ther. 2020;12:100.
37. Bateman RJ, Xiong C, Benzinger TL, Fagan AM, Goate A, Fox NC, Marcus DS, Cairns NJ, Xie X, Blazey TM, et al. Clinical and biomarker changes in dominantly inherited Alzheimer's disease. N Engl J Med. 2012;367:795–804.
38. Merlini M, Kirabali T, Kulic L, Nitsch RM, Ferretti MT. Extravascular CD3 + T Cells in Brains of Alzheimer Disease Patients Correlate with Tau but Not with Amyloid Pathology: An Immunohistochemical Study. Neurodegener Dis. 2018;18:49–56.
39. Balusu S, Horre K, Thrupp N, Snellinx A, Serneels L, Arranz IC, Sierksma AM, Simren A, Karikari J T, et al: **Long noncoding RNA MEG3 activates neuronal necroptosis in Alzheimer's disease**. *BioRxiv* 2022.
40. Lemaitre P, Tareem S, Pasciuto E, Mascali LG, Martirosyan A, Callaerts-Vegh Z, Dooley J, Holt MG, Yshii L, Liston A. **Molecular and cognitive signatures of ageing partially restored through synthetic delivery of IL2 to the brain** *BioRxiv* 2022.

Figures

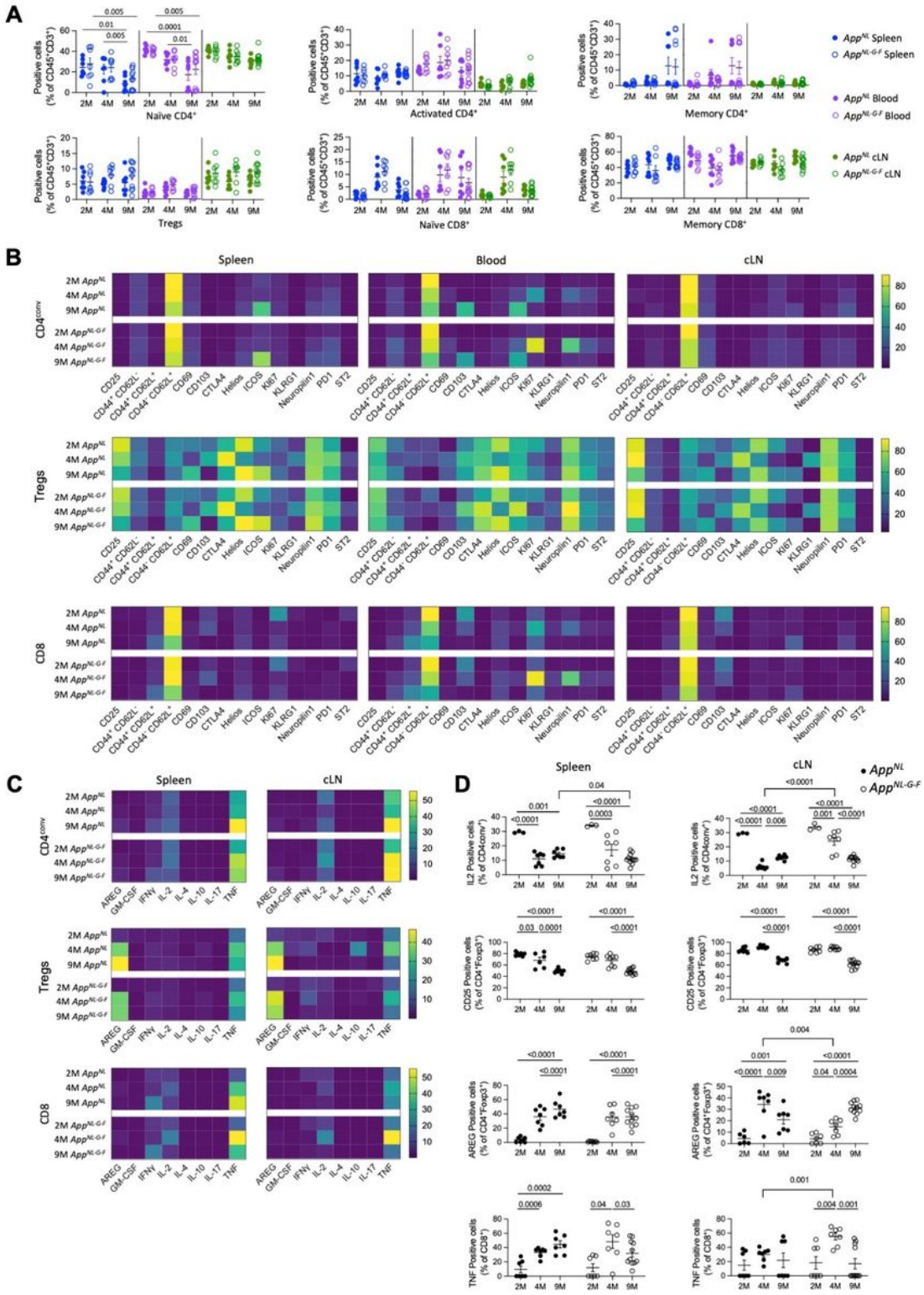

Figure 1

Cumulative age-dependent changes in the peripheral immunological compartments in *App*^{NL} and *App*$^{NL-G-F}$ mice. *App*^{NL} and *App*$^{NL-G-F}$ mice were assessed by high-dimensional flow cytometry for T cell immune profiles, at 2, 4 and 9 months of age. **A)** Frequency of main T cell populations in the spleen, blood, and cLN from *App*^{NL} and *App*$^{NL-G-F}$ mice (2 months: n=7,7; 4 months: n=7,7; 9 months: n=7, 11), as defined by tSNE projection (Supplementary Figure 1). **B)** Heatmaps displaying activation marker expression in

$CD4^{conv}$, Tregs, and CD8 subsets in spleen, blood, and cLN, for each genotype and age. **C)** Heatmaps displaying expression of cytokines in $CD4^{conv}$, Tregs, and CD8 subsets in spleen and cLN, for each genotype and age. **D**) Frequency of $IL2^+$ cells within $CD4^{conv}$ cells (2 months: n=3,3; 4 months: n=7,7; 9 months: n=7, 11), $CD25^+$ cells within Tregs (2 months: n=7,7; 4 months: n=7,7; 9 months: n=7, 11), and $AREG^+$ cells within Tregs (2 months: n=7,7; 4 months: n=7,7; 9 months: n=7, 11), measured by flow cytometry. Left column, Spleen; right column, cLN.

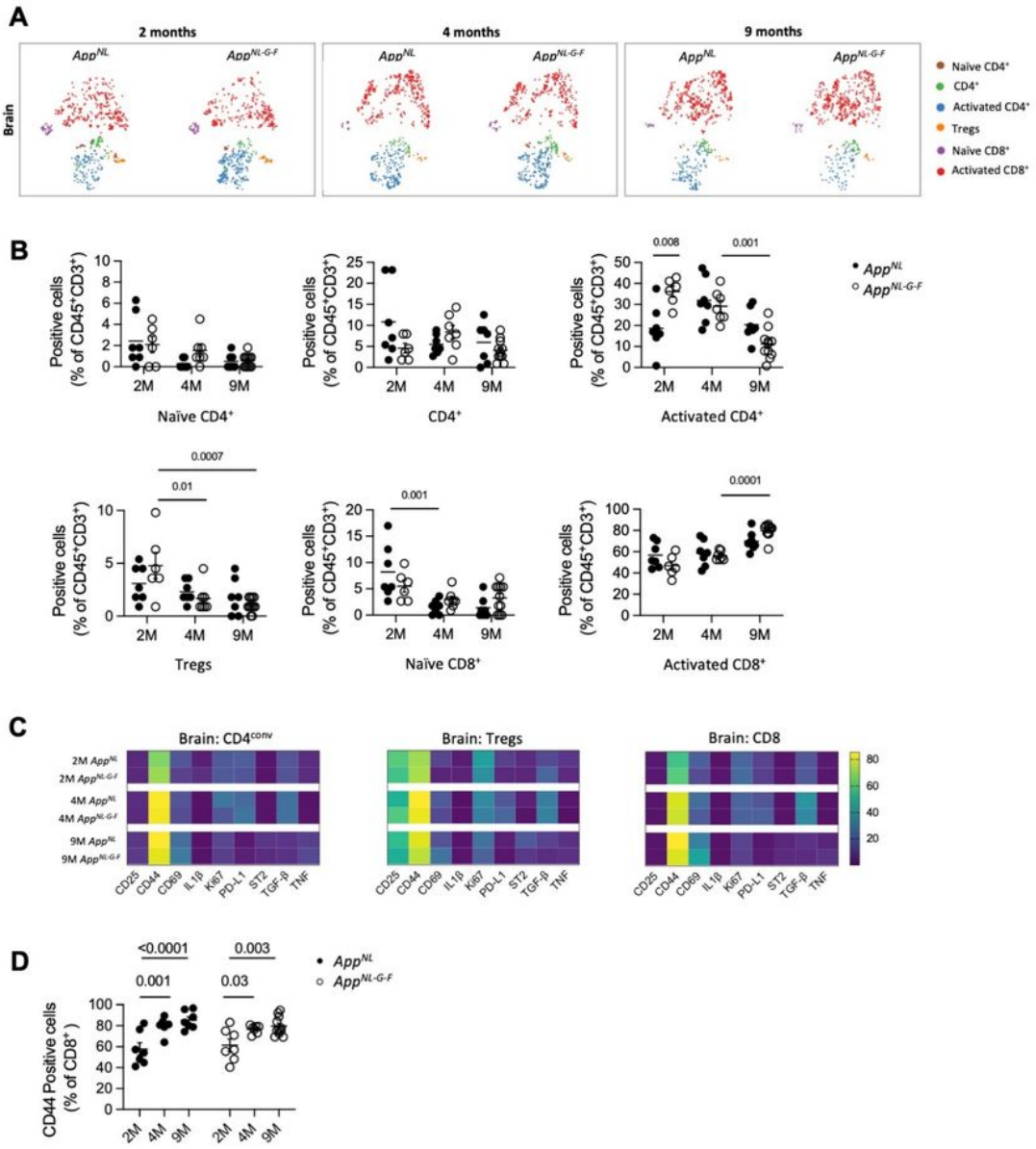

Figure 2

Cumulative age-dependent changes in the brain-resident immunological compartments in *App*^{NL} and *App*$^{NL-G-F}$ mice. A) Perfused mouse brains from *App*^{NL} and *App*$^{NL-G-F}$ mice were compared by high-dimensional flow cytometry to obtain the immune profiles of resident T cells, at 2 (n=7,7), 4 (n=7,7) and 9 (n=7,11) months of age. tSNE projection (4032 cells plotted) of the main T cell population clusters from concatenated samples. Immune populations were annotated based on expression of key protein markers, with **B)** cluster quantification. **C)** Heatmaps displaying the degree of expression for activation markers within the CD4^{conv}, Tregs, and CD8 populations in the brains of *App*^{NL} and *App*$^{NL-G-F}$ mice, at each age point. **D)** Frequency of CD44^{+} cells within the CD8 T cell population in the brain.

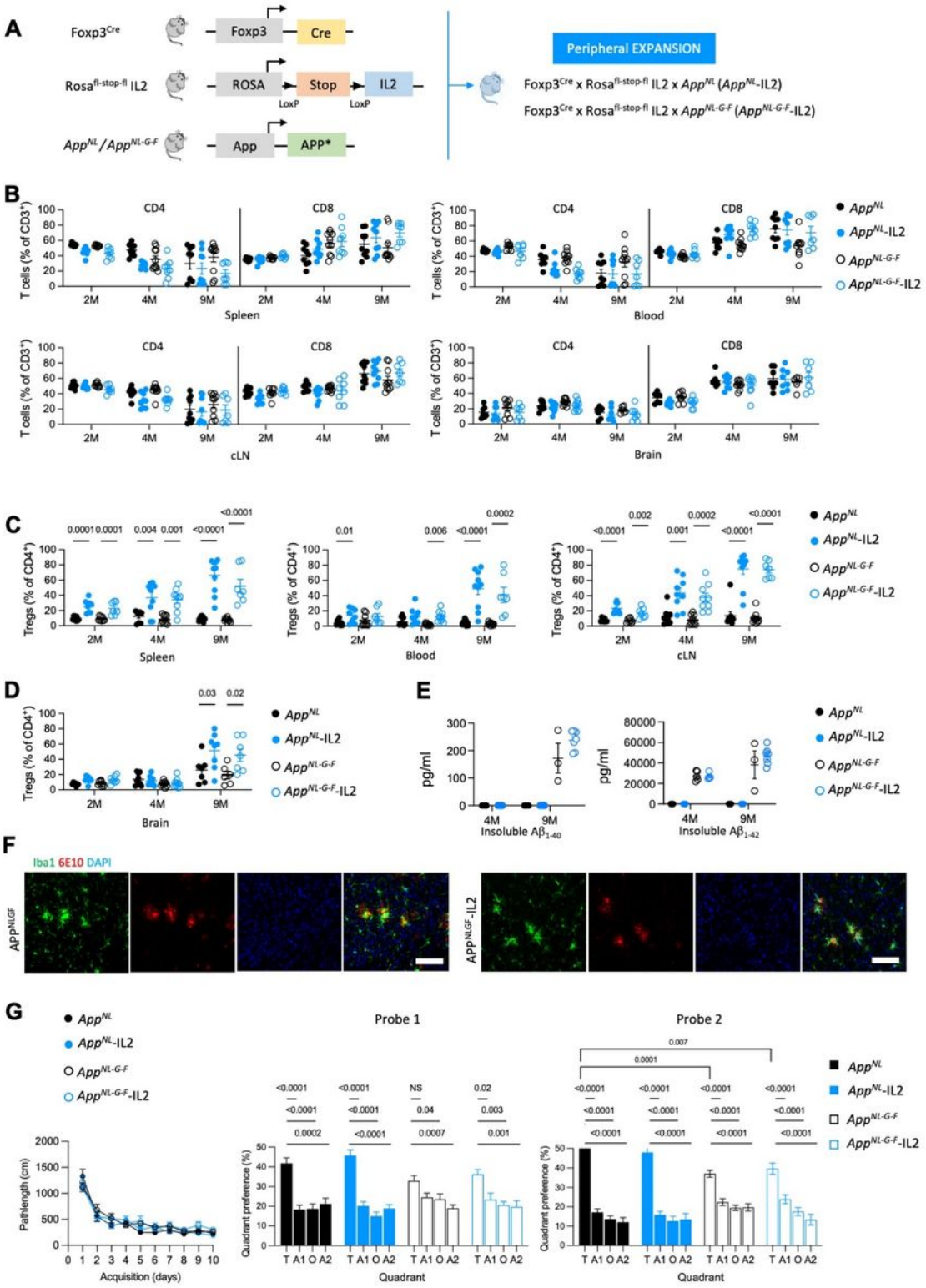

Figure 3

Peripherally-biased expansion of Treg numbers does not alter pathology of *App*$^{NL-G-F}$ mice. A) Schematic of the transgenic system employed for IL2 overexpression in Tregs in *App*^{NL} and *App*$^{NL-G-F}$ knock-in mice. **B)** Perfused mice (*App*^{NL}, *App*^{NL} –IL2, *App*$^{NL-G-F}$ and *App*$^{NL-G-F}$ –IL2 lines) were compared by high-dimensional flow cytometry to determine the immune profiles in the T cell population. Frequency of

$CD4^{conv}$ and CD8 T cells in spleen, blood and cLN at 2 (n=7,8,8,7), 4 (n=9,9,9,9) and 9 (n=9,10,10,7) months of age. Frequency of $CD4^{conv}$ and CD8 T cells in brain at 2 (n=7,8,8,7), 4 (n=9,9,9,9) and 9 (n=7,8,6,7) months of age. **C)** Frequency of Tregs in spleen, blood and cLN at 2 (n=7,8,8,7), 4 (n=9,9,9,9) and 9 (n=9,10,10,7) months of age. **D)** Frequency of Tregs in the brain at 2 (n=7,8,8,7), 4 (n=9,9,9,9) and 9 (n=7,8,6,7) months of age. **E)** ELISA measurements on levels of insoluble $Aß_{1-40}$ (left) and $Aß_{1-42}$ (right) extracted from whole cortex at 4 (n=5,5,5,4) and 9 (n=5,5,3,7) months of age. **F)** Representative cortical brain sections from 9 months old App^{NL-G-F} and App^{NL-G-F}-IL2 mice stained with anti-Iba1 and anti-Aß antibodies (6E10). Scale bar = 100 µm **G)** Spatial learning in the Morris Water Maze for App^{NL}, App^{NL} – IL2, App^{NL-G-F} and App^{NL-G-F} – IL2 lines (n= 12,12,22,14). Mice were tested at 9 months of age. Left: Path length to finding the hidden platform; Middle: Probe tests after 5 days (probe 1); Right: after 10 days (probe 2) of acquisition.

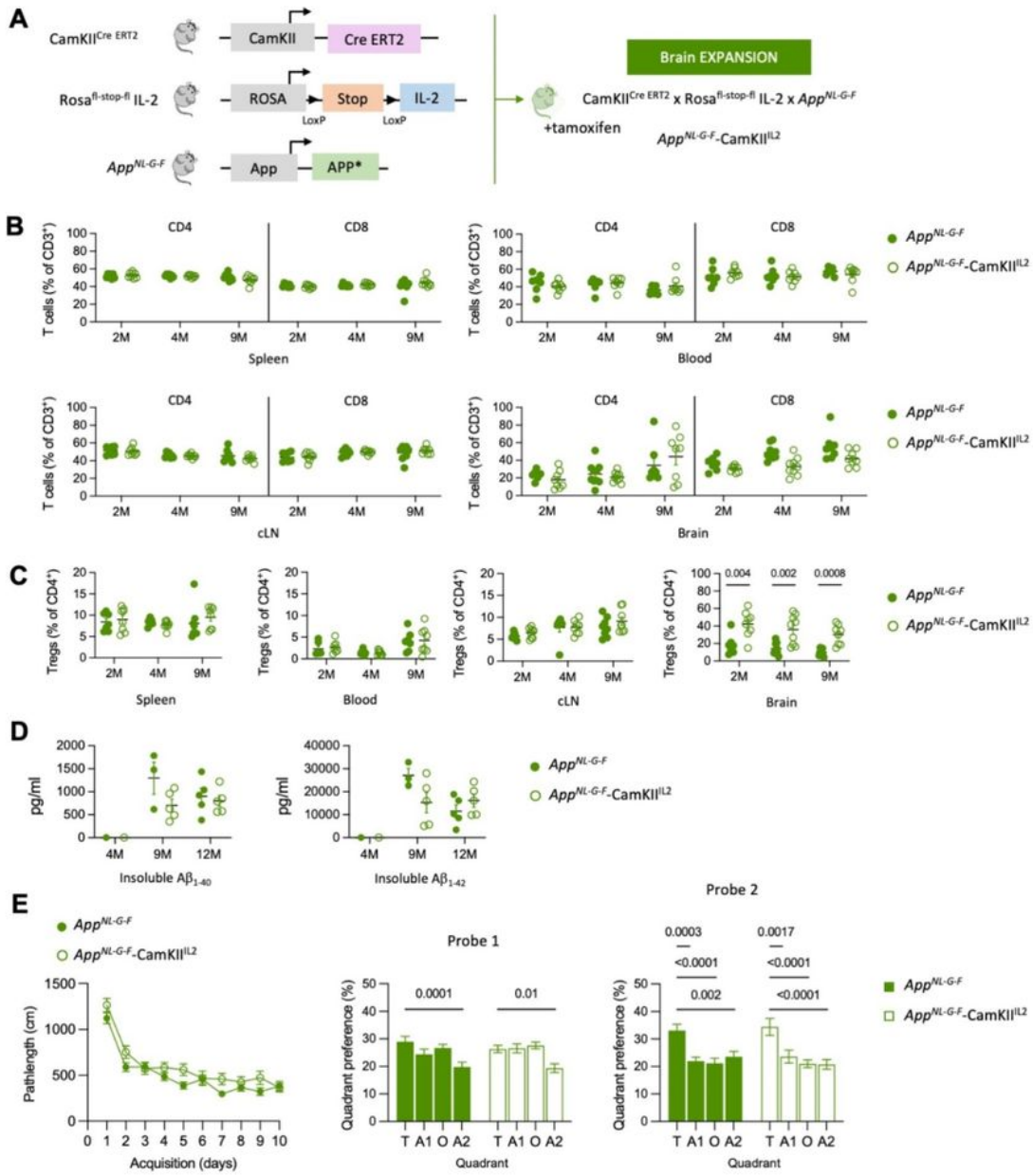

Figure 4

Brain-specific expansion of Treg numbers does not alter pathology in App knock-in mice. A) Schematic of the transgenic system employed for brain-specific IL2 expression in App knock-in mice. **B)** Perfused mice (*App*$^{NL-G-F}$ and *App*$^{NL-G-F}$ –CamK2^{IL2} lines) were compared by high-dimensional flow cytometry to determine the immune profiles in the T cell populations. Frequency of CD4^{conv} and CD8 T cells in spleen, blood and cLN at 2 (n=7,8), 4 (n=7,8) and 9 (n=8,8) months of age. Frequency of CD4^{conv} and CD8 T cells

in brain at 2 (n=7,8), 4 (n=9,9) and 9 (n=8,8) months of age. **C)** Frequency of Tregs in spleen, blood and cLN at 2 (n=7,8), 4 (n=7,8) and 9 (n=8,8) months of age. Frequency of Tregs in the brain at 2 (n=7,8), 4 (n=9,9) and 9 (n=8,8) months of age. **D)** ELISA measurements on levels of insoluble $Aß_{1-40}$ (left) and $Aß_{1-42}$ (right) at 4 (n=4,4), 9 (n=3,5) and 12 (n=5,5) months of age. **E)** Spatial learning in the Morris Water Maze for App^{NL-G-F} and App^{NL-G-F} –CamK2^{IL2} lines (n= 26,20). Mice were tested at 9 months of age. Left: Path length to finding the hidden platform; Middle: Probe tests after 5 days (probe 1); Right: after 10 days (probe 2) of acquisition.

Supplementary Files

This is a list of supplementary files associated with this preprint. Click to download.

- SupplementarymaterialMN.pdf